Conversion of Sox2-dependent Merkel cell carcinoma to a differentiated neuron-like phenotype by T antigen inhibition

Alexis Harold[a,1], Yutaka Amako[a,b,1], Junichi Hachisuka[c,d], Yulong Bai[e], Meng Yen Li[f], Linda Kubat[g], Jan Gravemeyer[g], Jonathan Franks[h], Julia R. Gibbs[a], Hyun Jung Park[e], Elena Ezhkova[f], Jürgen C. Becker[g], and Masahiro Shuda[a,b,2]

[a]Cancer Virology Program, Hillman Cancer Center, University of Pittsburgh Medical Center, Pittsburgh, PA 15213; [b]Department of Microbiology and Molecular Genetics, University of Pittsburgh, Pittsburgh, PA 15219; [c]Pittsburgh Center for Pain Research, University of Pittsburgh, Pittsburgh, PA 15213; [d]Department of Neurobiology, University of Pittsburgh, Pittsburgh, PA 15213; [e]Department of Human Genetics, University of Pittsburgh, Pittsburgh, PA 15260; [f]The Tisch Cancer Institute, Black Family Stem Cell Institute, Department of Cell, Developmental, and Regenerative Biology, Icahn School of Medicine at Mount Sinai, New York, NY 10029; [g]Translational Skin Cancer Research, Dermatology, German Cancer Consortium (DKTK), 45141 Essen, Germany; and [h]Center for Biologic Imaging, University of Pittsburgh, Pittsburgh, PA 15261

Edited by Thomas E. Shenk, Princeton University, Princeton, NJ, and approved August 21, 2019 (received for review April 29, 2019)

Viral cancers show oncogene addiction to viral oncoproteins, which are required for survival and proliferation of the dedifferentiated cancer cell. Human Merkel cell carcinomas (MCCs) that harbor a clonally integrated Merkel cell polyomavirus (MCV) genome have low mutation burden and require viral T antigen expression for tumor growth. Here, we showed that MCV$^+$ MCC cells cocultured with keratinocytes undergo neuron-like differentiation with neurite outgrowth, secretory vesicle accumulation, and the generation of sodium-dependent action potentials, hallmarks of a neuronal cell lineage. Cocultured keratinocytes are essential for induction of the neuronal phenotype. Keratinocyte-conditioned medium was insufficient to induce this phenotype. Single-cell RNA sequencing revealed that T antigen knockdown inhibited cell cycle gene expression and reduced expression of key Merkel cell lineage/MCC marker genes, including *HES6*, *SOX2*, *ATOH1*, and *KRT20*. Of these, T antigen knockdown directly inhibited Sox2 and Atoh1 expression. MCV large T up-regulated Sox2 through its retinoblastoma protein-inhibition domain, which in turn activated Atoh1 expression. The knockdown of Sox2 in MCV$^+$ MCCs mimicked T antigen knockdown by inducing MCC cell growth arrest and neuron-like differentiation. These results show Sox2-dependent conversion of an undifferentiated, aggressive cancer cell to a differentiated neuron-like phenotype and suggest that the ontology of MCC arises from a neuronal cell precursor.

phenotypic conversion | Merkel cell polyomavirus | Merkel cell carcinoma | Sox2 | Atoh1

Several types of cancer cells, specifically those that are addicted to a given oncogene activation or tumor-suppressor inactivation for tumorigenesis, revert from their malignant state to normal state when the key oncogene is inhibited or tumor suppressor is restored (1–3). The reversion of a malignant phenotype has been often seen in cancer cells transformed by tumor viruses. In various experimental models, cells transformed by tumor viruses, such as Rous sarcoma virus and animal polyomaviruses like SV40, are addicted to viral oncogene expression and have been shown to revert to the original uninfected cells when the viral oncoprotein is inhibited (4–6).

Merkel cell polyomavirus (MCV; MCPyV) is the most recently identified human oncogenic polyomavirus that causes ∼80% of Merkel cell carcinoma (MCC). MCV is clonally integrated in the MCC tumor genome, which results in the persistent expression of viral T oncogene in tumor cells (7). Similar to other polyomaviruses, MCV T antigen encodes 2 major transcripts that express large T (LT) and small T (sT) proteins. Viral sequence analysis in MCC tumors showed that integrated LT antigens are C-terminally truncated by tumor-specific polymorphisms, resulting in the loss of viral replication capacity (8). Functional studies of sT and tumor-derived LT antigens confirmed their tumorigenic potential (9). As seen in SV40-immortalized cells, MCV$^+$ MCC tumor cells show an oncogenic addiction to viral oncogene expression: The inhibition of T antigen expression by T antigen knockdown induces cell cycle arrest and nonapoptotic cell death (10), which also leads to a loss of tumorigenicity in nude mice (11). However, a detailed analysis of the MCC cells that lose T antigen expression has not been performed yet.

MCV$^+$ MCCs have a lower mutation burden than MCV$^-$ MCC and maintain a relatively intact genetic profile (12). Similar to other virus-induced tumors, while p53 and retinoblastoma protein (Rb) tumor-suppressor genes remain wild-type in MCV$^+$ MCC tumors (13, 14), their functions are likely to be suppressed directly or indirectly by the viral T antigen oncogene. This is supported by the fact that MCC tumorigenesis depends on viral T antigen expression and does not require a complex selection of genetic mutations that favor cancer cell proliferation. Based on these observations, we hypothesized that virus-positive MCC cancer

Significance

Normal cells can be transformed into cancer cells by viral oncogenes. Reversion of a viral human cancer cell, however, into a differentiated cell by viral oncogene inhibition has not been described. Merkel cell carcinoma (MCC) is a neuroendocrine cancer caused by Merkel cell polyomavirus (MCV) that encodes a T antigen oncogene. When MCV$^+$ MCC cells with T antigen knockdown are cocultured with keratinocytes, the MCC phenotype converts to a differentiated neuronal phenotype and loses Merkel cell factor Sox2 and Atoh1 expression. MCV large T activates Sox2 and Atoh1 by its ability to inhibit retinoblastoma. Sox2 inhibition similarly induced this phenotypic conversion of MCC. These findings suggest that MCV induces cancer by dysregulating embryonic Merkel cell differentiation pathways.

Author contributions: A.H., Y.A., J.H., H.J.P., E.E., J.C.B., and M.S. designed research; A.H., Y.A., J.H., Y.B., M.Y.L., L.K., J.G., J.F., J.R.G., H.J.P., E.E., J.C.B., and M.S. performed research; A.H., Y.A., J.H., Y.B., M.Y.L., L.K., J.G., J.F., J.R.G., H.J.P., E.E., J.C.B., and M.S. analyzed data; and Y.A., J.H., Y.B., M.Y.L., J.G., J.F., H.J.P., E.E., J.C.B., and M.S. wrote the paper.

The authors declare no conflict of interest.

This article is a PNAS Direct Submission.

Data deposition: The single-cell sequence dataset reported in this paper has been deposited in the Gene Expression Omnibus (GEO) database, https://www.ncbi.nlm.nih.gov/geo/ (accession no. GSE136867).

[1]A.H. and Y.A. contributed equally to this work.

[2]To whom correspondence may be addressed. Email: mas253@pitt.edu.

This article contains supporting information online at www.pnas.org/lookup/suppl/doi:10.1073/pnas.1907154116/-/DCSupplemental.

First published September 16, 2019.

cells may retain the capacity to be reverted into an untransformed state by T antigen inhibition.

In the present study, in order to study the fate of MCC cancer cells after the viral oncogene deprivation, we performed genetical and cell biological analyses on MCV$^+$ MCC cells with viral T antigen knockdown. We found that in vitro T antigen knockdown in MCV$^+$ MCC cells with cocultured human keratinocytes alters its round suspension cell morphology to adherent cell morphology and confers neuronal phenotypes, including neurite outgrowth, cytosolic vesicle accumulation, and sodium channel-dependent excitability. MCC are neuroendocrine tumors with morphologic and immunophenotypic similarities to Merkel cells (15). Transcriptional profiling of the Merkel cells in mouse skin showed that these cells express neuronal transcription factors, presynaptic molecules, and ion-channel subunits (16, 17). Of them, Atoh1 and Sox2 are critical transcription factors for Merkel cell development, in which Atoh1 plays a role in Merkel cell specification, while Sox2 controls Merkel cell maturation (18–21). Our single-cell RNA sequencing study demonstrated that the inhibition of viral T antigen in MCC cells enforces cell cycle exit, shutting off cell cycle-associated gene expression, and simultaneously decreases the expression of the key Merkel cell lineage factors and MCC markers, including Sox2 and Atoh1. We found that viral LT is responsible for the Sox2 activation and that Sox2 is a direct upstream transcriptional activator of *ATOH1*. Finally, the Sox2 knockdown study revealed that Sox2 plays a critical role in both MCV$^+$ MCC cell proliferation and maintenance of the MCC phenotype. Our data demonstrate that MCV-associated human MCC is a human cancer that can revert to an untransformed state and acquire a differentiated neuron-like phenotype, and that the viral activation of Sox2 serves as a key switch for this phenotypic conversion.

Results

MCV T Antigen Knockdown in MCV$^+$ MCC Cells Promotes Morphological Alteration with Cocultured Keratinocytes. Merkel cells localize to the basal layer of the epidermis and are in direct association with keratinocytes. To mimic Merkel cells or MCC growth in situ, we cocultured MCV$^+$ MCC cells with human keratinocytes. We initially used MCV$^+$ MCC cells MKL-1, MKL-2, MS-1, WaGa, and CVG-1 (10, 22), which grow in suspension culture, forming loose clusters when cultured in the standard 10% FCS RPMI medium or keratinocyte growth medium (*SI Appendix*, Fig. S1*A*). When cocultured with human keratinocytes in the keratinocyte growth medium, the MCC cells became disaggregated into round cells, and a subset of the cells attached to the cell culture dishes. Cocultured keratinocytes were distinguished from MCC cells based on the large cell size and intracellular granules seen in the differentiated keratinocytes. Among the attached MCC cells, we observed morphologically distinct MCC cells with cytoplasmic projections. This morphological alteration was not seen in MCC cells grown with the conditioned medium from the keratinocyte culture or in transwell cocultured MCC cells with keratinocytes, suggesting that secreted factors from keratinocytes are not sufficient to induce morphological changes in MCC cells (*SI Appendix*, Fig. S1*B*). This outgrowth of cellular processes was observed most frequently in CVG-1, followed by MKL-2 and MS-1 cells. We tested whether MCV T antigen expression affects this morphological alteration by using a lentiviral short-hairpin RNA (shRNA) that targets all T antigen isoforms (10, 23). For the rest of the experiments, we used MS-1 and CVG-1 cells, early-passage cell lines established by our group (22, 24), and MKL-2 cells, an extended-passage cell line established by Martin et al. (25) prior to the discovery of MCV (10). These MCV$^+$ MCC cell lines were transduced with GFP-expressing control shRNA (shCtrl-eGFP) or shpanT-eGFP that targets all T antigen isoform transcripts, and then the shRNA-transduced cells were cocultured with keratinocytes. After 5 d of coculture, cell morphology was evaluated under a fluorescence microscope. T antigen knockdown in MS-1, MKL-2, and CVG-1 cells significantly increased the number of eGFP$^+$ cells displaying short and large cellular projections (Fig. 1*A* and *SI Appendix*, Fig. S1*C*). Immunofluorescence staining confirmed that the projections are neurofilament L$^+$ (NFL$^+$) neurites in most of the shpanT-transduced MS-1 and CVG-1 cells (83.7 ± 2.7% and 86.5 ± 2.7%, $P < 0.05$ for MS-1 and CVG-1, respectively) (Fig. 1*B* and *SI Appendix*, Fig. S1*D*). We graded the neurite outgrowth on a scale of 0 to 3 according to the presence of the cellular process and the length of projections relative to a cell size (*SI Appendix*, Fig. S1*E*). Cells with longer, polarized grade 2 and 3 projections were significantly increased by T antigen knockdown in all 3 MCV$^+$ MCC cells examined (Fig. 1*C*). Bromodeoxyuridine (BrdU) labeling experiments in cocultured CVG-1 and MS-1 cells demonstrated that T antigen knockdown ablates the BrdU$^+$ MCC cells irrespective of cellular neurite-positivity, while some keratinocytes incorporate BrdU (*SI Appendix*, Fig. S1 *F* and *G*). These data are consistent with our previous results showing that T antigen knockdown induces G0/G1 arrest (10). We also examined the ultrastructure of the neurite$^+$ MS-1 and MKL-2 cells by electron microscopy (Fig. 1*D* and *SI Appendix*, Fig. S1*H*). The focal accumulation of dense core vesicles transported outward along cellular projection was detected in shpanT-transduced MS-1 and MKL-2 cells, while vesicles scattered in the cytoplasm were seen in shCtrl-transduced cells, confirming that the mature neural phenotype is conferred by T antigen knockdown in MCV$^+$ MCC cells. The expression of cholecystokinin, a synaptic neuropeptide that is expressed in neuroendocrine Merkel cells as well as neurons (16, 26, 27), was significantly induced in MKL-2 and CVG-1 cells by T antigen knockdown (Fig. 1*E*).

Neurite$^+$ MCV T Antigen Knockdown MCC Cells Fire Na$^+$-Dependent Action Potentials. To test the physiological property of the differentiated MCC cells induced by T antigen knockdown, we performed whole-cell patch-clamp recordings in MS-1 cells. Resting membrane potentials ranged from −60 to −70 mV. None of the control MCC cells showed action potential upon current injection (Fig. 2*A*) ($n = 9$). In contrast, in the majority of shpanT-transduced MS-1 cells (83%) displaying grade 3 neurite outgrowth, the action potentials can be detected and blocked by treatment with tetrodotoxin (TTX), a neurotoxin that inhibits neuronal excitability by binding to voltage-gated sodium channels (Fig. 2*B*) ($n = 12$, χ^2 test $P = 0.0002$ between shCtrl and shpanT-transduced MS-1 cells). When compared to a representative recording from a dorsal root ganglion neuron, however, action potentials from differentiated MS-1 cells do not exhibit clear afterhyperpolarization (*SI Appendix*, Fig. S2*A*). All responsive cells showed only a single spike upon current injection ($n = 10$). Since Merkel cells fire Ca^{2+}-action potentials (28), we examined if Ca^{2+} is involved in these action potentials by using artificial cerebrospinal fluid (ACSF) with or without calcium depletion. TTX completely blocked action potentials, irrespective of calcium depletion (Fig. 2 *C* and *D*). Calcium-free ACSF did not block action potentials (Fig. 2*D*), indicating that voltage-gated sodium channels, but not voltage-gated calcium channels, mediate this action potential. Consistent with this function, among the 5 voltage-gated sodium channel genes (*SCN*) examined, T antigen knockdown up-regulated the expression of*SCN3A* and *SCN9A* in MS-1 cells (Fig. 2*E*). In MKL-2 cells and CVG-1 cells, 4 SCN genes—including *SCN1A*, *SCN2A*, *SCN3A*, and *SCN9A*—were coordinately induced by shpanT (Fig. 2*E* and *SI Appendix*, Fig. S2*B*). *SCN8A* was unchanged in all 3 MCC cell lines (Fig. 2*E* and *SI Appendix*, Fig. S2*B*). Since the nature of action potentials detected in the neurite$^+$ MS-1 cells differs from that in normal Merkel cells, the

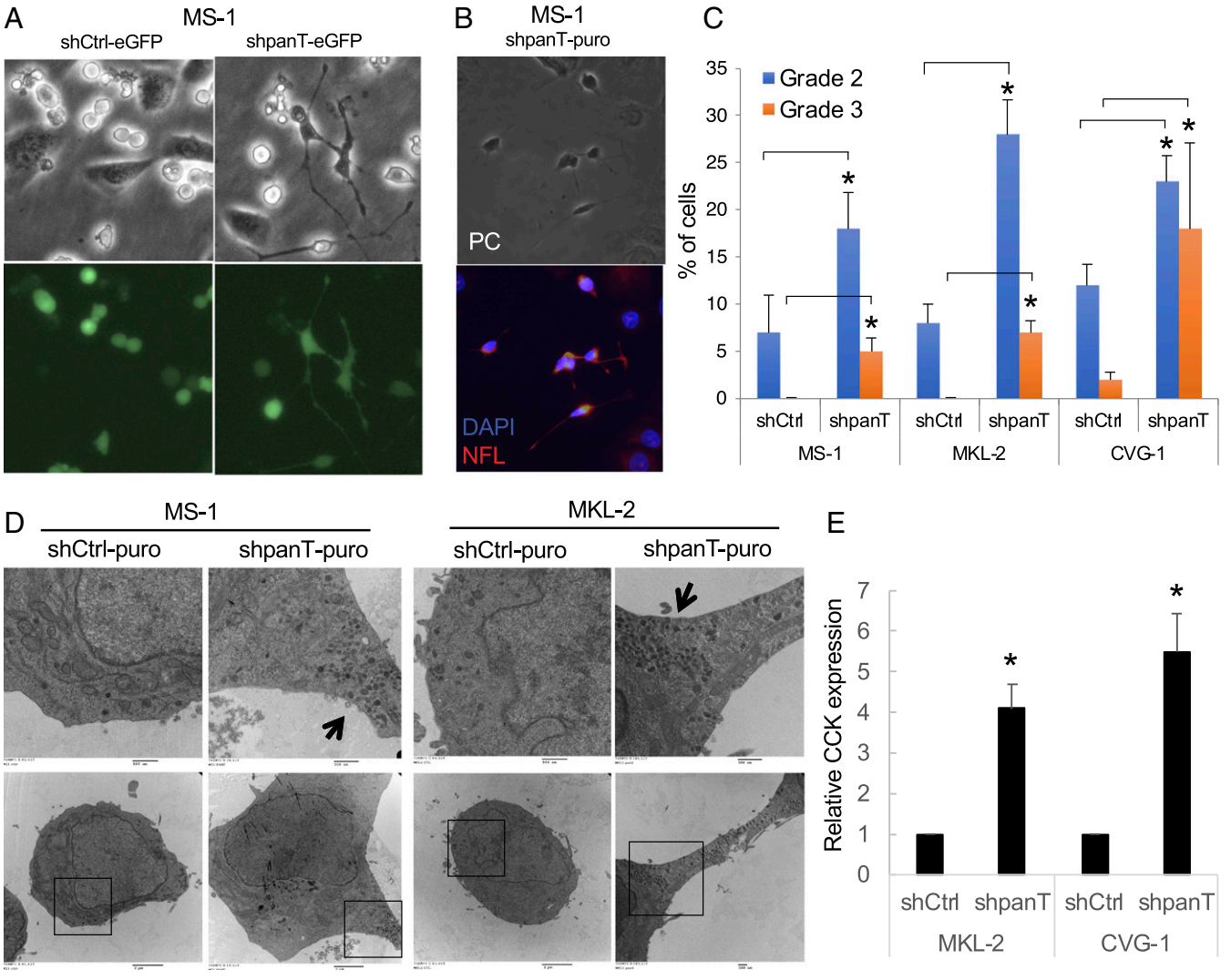

Fig. 1. MCV T antigen knockdown promotes the morphological alteration of MCC tumor cells into cells with a neurite structure in the presence of cocultured keratinocytes. (*A*) MS-1 cells were transduced with GFP-coding shRNA, targeting all T antigen isoforms (shpanT-eGFP) and control shRNA (shCtrl-eGFP) for 3 d, and then cocultured with human primary keratinocytes for 5 d. GFP$^+$ MCC cells with T antigen knockdown exhibit distinct cytoplasmic projections. (Magnification: 40×.) (*B*) Immunofluorescence staining of NFL using MS-1 cells with shpanT-puro, the cytoplasmic projections are NFL$^+$ neurite. (Magnification: 40×.) (*C*) T antigen knockdown increases cells with elongated neurite structures (grades 2 and 3) in 3 MCV$^+$ MCC cells. The neurite formation was graded from 0 to 3 (*SI Appendix*, Fig. S1*E*). Grade 0 represents no process, grade 1 cellular process-positive, grade 2 polarized projections, and grade 3 with projection a longer than 2-cell body sizes. Data are shown as average ± SE, $*P < 0.05$ (Student *t* test). (*D*) The production of dense core vesicles at the cellular projection in neurite$^+$ MCC cells. MS-1 and MKL-2 cells transduced with shCtrl-puro or shpanT-puro were puromycin-selected and subjected to observations by a transmission electron microscopy. The arrow indicates dense core neuroendocrine granules shown in the magnified region. (*E*) T antigen knockdown increases cholecystokinin (CCK) expression in MKL-2 and CVG-1 cells. The CCK mRNA expression was determined by qRT-PCR and normalized with the18S ribosomal RNA control by the $2^{-\Delta\Delta CT}$ method. Data are shown as average ± SD, $*P < 0.05$ (Student *t* test).

neurite$^+$ cells induced from MCV$^+$ MCC by T antigen knockdown resemble neurons rather than Merkel cells.

The Loss of Viral T Antigen Down-Regulates Cell Cycle Genes and Merkel Cell/MCC Marker Genes in MCV$^+$ MCC Cells. In order to investigate the genetic changes associated with the morphological alteration in MCC cells, we performed single-cell RNA sequencing using keratinocyte-cocultured CVG-1 cells with or without T antigen knockdown (29). The cocultured CVG-1 cells transduced with shpanT showed increased neurite formation as compared to those with shCtrl when harvested (*SI Appendix*, Fig. S3*A*). Even though the coculture was initiated with an equal number of keratinocytes and CVG-1 cells, the overall density of the shpanT-transduced cells was lower than the shCtrl cells due to the growth arrest induced by T antigen knockdown.

The t-distributed stochastic neighboring (t-SNE) plot was generated from 2 libraries derived from 8,766 keratinocyte-cocultured shCtrl- and 9,456 shpanT-transduced CVG-1 cells (Fig. 3*A*). It consists of 3 independent clusters (I ~ III), in which cluster I contains a majority of the shCtrl dataset, while cluster II is composed of the shpanT dataset. Cluster III is a mixture of the shCtrl and shpanT datasets. To analyze the difference in gene-expression pattern in every single cell, we employed the *k*-clustering algorithm and obtained 6 well-separated clusters (Fig. 3 *A*, *Right* and *SI Appendix*, Fig. S3*B*). Cluster numbers are given based on the cluster size. Clusters 1 (C1), C2, C4, and C5 expressed MCC marker genes *CHGA* (chromogranin A) and *SYP* (synaptophysin), while C3 highly expressed the keratinocyte marker gene *KRT14* (Fig. 3*B*). This indicates that C3 is a dataset derived from cocultured keratinocytes and that other clusters

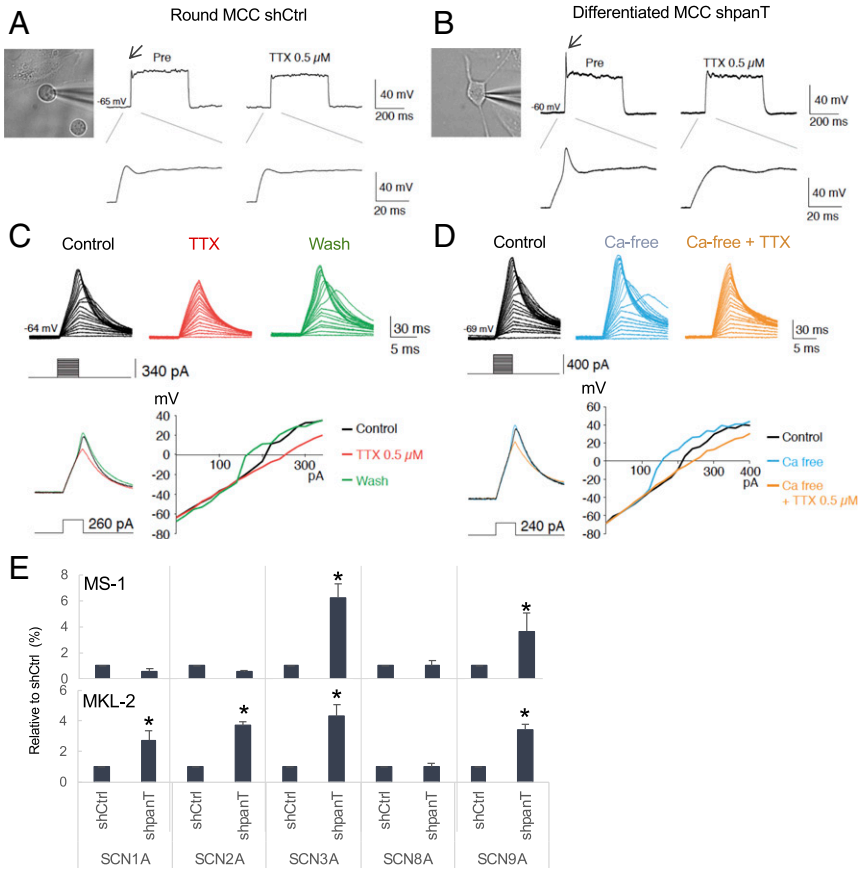

Fig. 2. Neurite^{+} MCC cells display neuronal, but not Merkel cell electrophysiological properties. (*A*) Representative trace of an MS-1 cell transduced with shCtrl-puro. (Magnification: 40×.) Current injection (180 pA, 400 ms) did not cause action potentials (*Left*). TTX application had no effect (*Right*). (*B*) Sample trace of an MS-1 cell transduced with shpanT-puro that displays grade 3 differentiation. Current injection (120 pA, 400 ms) caused an action potential (arrow, left) that was blocked by TTX (0.5 μM). (*C*) The effect of TTX on the action potential of a shpanT-puro–transduced MCC cell. Step pulses from 0 to 340 pA were applied. Action potentials observed in the control sample (black) were completely blocked by TTX (red). A TTX washout restores action potentials (green). The current–voltage relationship is shown in a graph. (*D*) The effect of Ca-free ACSF on the action potentials of a Pan-T treated MCC cell. Step pulses from 0 to 400 pA were applied. Action potential is not blocked by Ca-free ACSF (light blue), but additional TTX does block the action potential in the absence of calcium (orange). (*E*) Voltage-dependent sodium channel genes (*SCN*) are up-regulated by T antigen knockdown in MCV^{+} MS-1 and MKL-2 cells. qRT-PCR was performed for SCN1A, SCN2A, SCN3A, SCN8A, and SCN9A, and relative expression to shCtrl transduced cells was determined by the $2^{-\Delta\Delta CT}$ method with the18S ribosomal RNA control. Data are shown as average ± SD, $^{*}P < 0.05$ (Student *t* test).

represent a dataset from MCV^{+} CVG1 cells. MCV T antigen expression was predominantly detected in C2, C4, and C5, which overlaps with the dataset from the shCtrl library in cluster I (Fig. 3 *A*, *Left* and Fig. 3*C*). On the other hand, MCV T antigen mRNA expression is markedly lower in C1, which overlaps with the dataset from the shpanT library in cluster II (Fig. 3 *A*–*C*). This result is consistent with efficient T antigen knockdown by shpanT. Similar to C1, C6 and the keratinocyte-derived C3 do not express MCV T antigen. While the majority of C6 consists of the shCtrl dataset, T antigen expression was undetectable, and the expression of both MCC and keratinocyte markers was low (Fig. 3*B*). Because of the unclear cellular identity and the relatively small cluster size, we excluded C6 from the current analysis together with C3. Nonetheless, the clear separation of cluster I and cluster II in t-SNE indicates that T antigen knockdown significantly alters the cellular transcriptome in CVG-1 cells.

To further define C2, C4, and C5, we examined cell cycle marker expression. C4 expresses G1/S-phase cell cycle markers, including *CCNE1*, *CDK2*, and *E2F1*, while C5 is positive for S- and G2/M-phase markers, including *CCNA2*, *CCNB1*, *MKI67*, and *AURKA* (Fig. 3 *B*, *Right* and *SI Appendix*, Fig. S3*C*). The expression of these cell cycle marker genes is nearly absent in C1 and C2. Accordingly, we defined C1 to be noncycling CVG-1 cells with T antigen knockdown, and C2 to be noncycling CVG-1 cells with control shRNA. C4 and C5 represent cycling CVG-1 control cells that commit G1/S and S/G2/M cell cycle phases, respectively.

In order to study the gene-expression changes associated with T antigen knockdown in CVG-1 cells, a differential gene expression (DE) analysis was performed between clusters C2/C4/C5 and C1 (*SI Appendix*, Fig. S3*D* and Dataset S1). To validate our DE analysis, we examined previously reported E2F target genes (30), because MCV LT has been shown to activate E2F by inhibiting Rb in MCC cells (31, 32). Among the 65 E2F target genes expressed in C1, C2, C4, and C5, 60 genes showed negative log fold-change (logFC) values in C1, suggesting that E2F target genes are coordinately suppressed by T antigen knockdown (*SI Appendix*, Fig. S3*D* and Dataset S1). In line with this result, canonical E2F target genes—including *CCNE1*, *E2F1*, *CDK2*, *CCNA2*, and *MKI67*—were suppressed in C1 and C2 (Fig. 3*B* and *SI Appendix*, Fig. S3*C*). This is consistent with the restoration of Rb tumor-suppressor activity in T antigen knockdown cells. Of 5 E2F targets up-regulated in C1, 3 genes were AP1 genes: *FOS, JUNB*, and *JUN* (*SI Appendix*, Fig. S3*D* and Dataset S1). Neuronal transmitters and transsynaptic stimulation activate AP1 genes in neuronal cells (33). While the mediator is

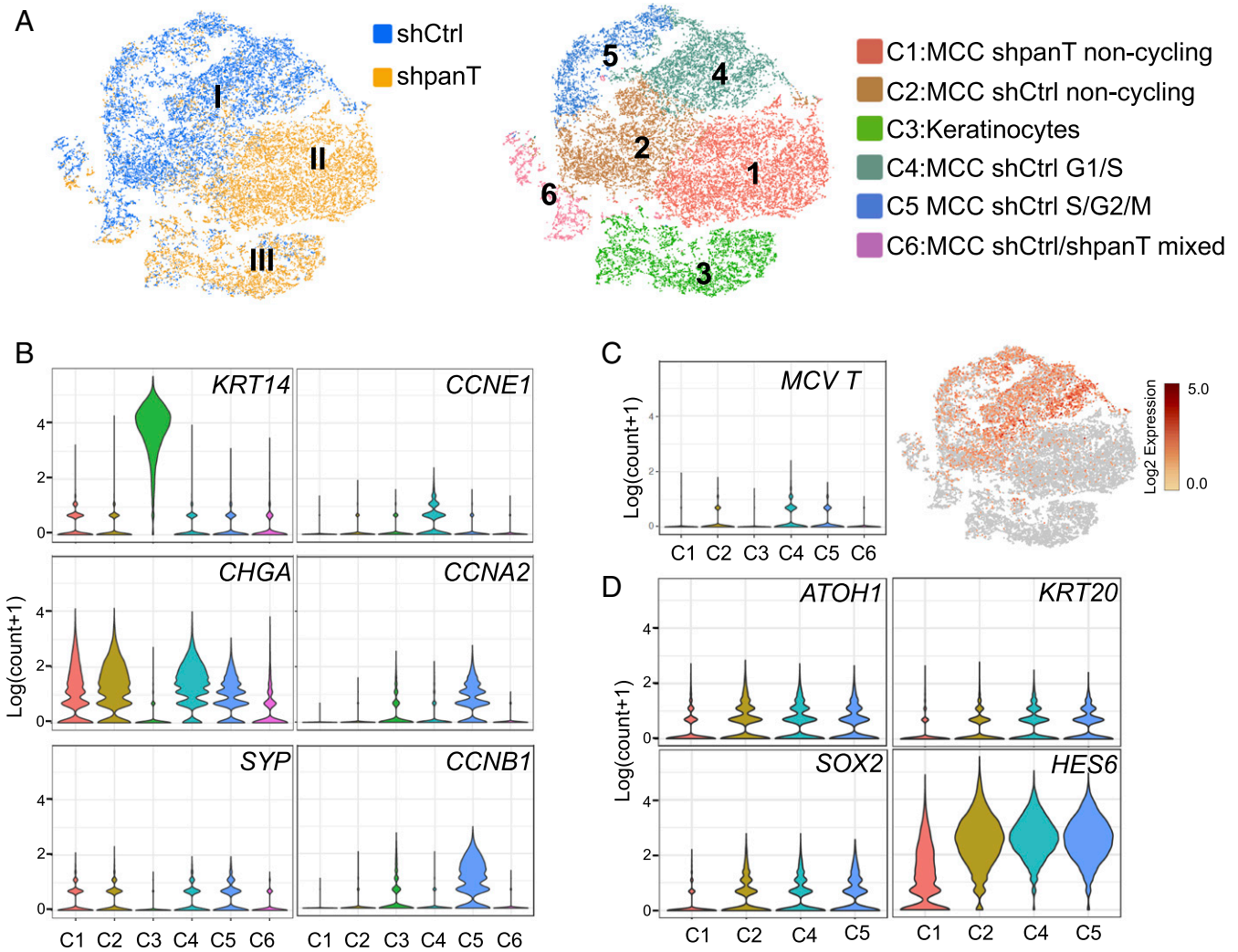

Fig. 3. T antigen inhibition in MCV$^+$ MCC cells ablates cell cycle-associated gene expression and decreases MCC and Merkel cell marker gene expression. (*A*) t-SNE plot visualizing the datasets from shCtrl (blue) and shpanT (brown) single-cell sequencing libraries (*Left*). t-SNE plot visualizing 6 (C1 ~ C6) cluster assignments of cells defined by *k*-clustering (*Right*). (*B*) Violin plots showing the distributions of the log-transformed average count of various marker genes in each cell cluster. Keratinocyte (*KRT14*) and MCC (*CHGA*, and *SYP*) marker-gene expression defined C1, C2, C4, C5, and C6 as CVG-1 cells, and C3 as keratinocytes. Cell cycle marker-gene expression analysis also defined C1, C2, and C6 as noncycling CVG-1 cells, and C4 and C5 as cycling CVG-1 cells in G1/S and in S/G2/M, respectively. (*C*) A Violin plot (*Left*) illustrating the distribution of MCV T antigen expression in each cell cluster. Plot (*Right*) maps the $\log_2$-transformed counts to a t-SNE result. (*D*) Violin plots illustrating the distributions of expression of Merkel cell and MCC marker genes in C1, C2, C4, and C5.

unknown, the activation of AP1 genes in the T antigen knockdown cells may represent the activated neuronal activities. Although both C1 and C2 are datasets from noncycling cells, a clear separation of noncycling C1 and C2 clusters on the t-SNE indicates that T antigen knockdown in CVG-1 cells results in cell cycle exit and further alters the transcriptome, which is even distinct from noncycling shCtrl cells.

In the DE analysis, we also investigated MCC marker genes (34–37) and Merkel cell marker genes, which have been previously characterized in Atoh1$^+$ mouse Merkel cells as compared to Atoh1$^-$ epidermal cells (16, 17). Atoh1 is the Merkel cell lineage-determining transcription factor, which is essential for Merkel cell development in mouse skin (18, 38). Merkel cell transcription factors *ATOH1*, *SOX2*, *HES6*, and MCC marker *KRT20* showed negative logFC values as expressed lowly in C1 in comparison to C2/C4/C5 (*SI Appendix*, Fig. S3*D* and Dataset S1). Violin plots also confirmed that cells that highly express these 4 genes are markedly reduced in C1 (Fig. 3*D*). This reduction is not a simple result of cell cycle exit by T antigen knockdown, because the expression of these genes is also detected in C2 derived from noncycling shCtrl CVG-1 cells (Fig. 3*D*). In addition to these 4 markers, *ENO2*, *BCL2*, *PAX5*, and *CD99* reported to be overexpressed in MCC cells (34–37) were also down-regulated in C1 (*SI Appendix*, Fig. S3*E*). In contrast, other known Merkel cell genes related to synaptic release machinery—such as *CADPS*, *CPE*, *PCSK*, and *SNAP25*—were unchanged or slightly increased in C1 (*SI Appendix*, Fig. S3 *D* and *F*), consistent with active secretory vesicle accumulation in neurite$^+$ MCC cells (*SI Appendix*, Fig. S3*F*). Neurite and axonal markers, including neurofilament L (*NEFL*) and Tau (*MAPT*), were also slightly increased in C1 by T antigen knockdown. These data indicate that genes expressed in Merkel cells and MCC are down-regulated by viral T antigen knockdown, whereas markers involved in neurosecretory functions are sustained or even increased.

Viral T Antigen Maintains Expression of Merkel Cell Lineage Makers, Sox2 and Atoh1 in MCC. Single-cell RNA sequencing data suggest that Merkel cell lineage markers Sox2 and Atoh1, which play important roles in mouse Merkel cell development (18–21), are

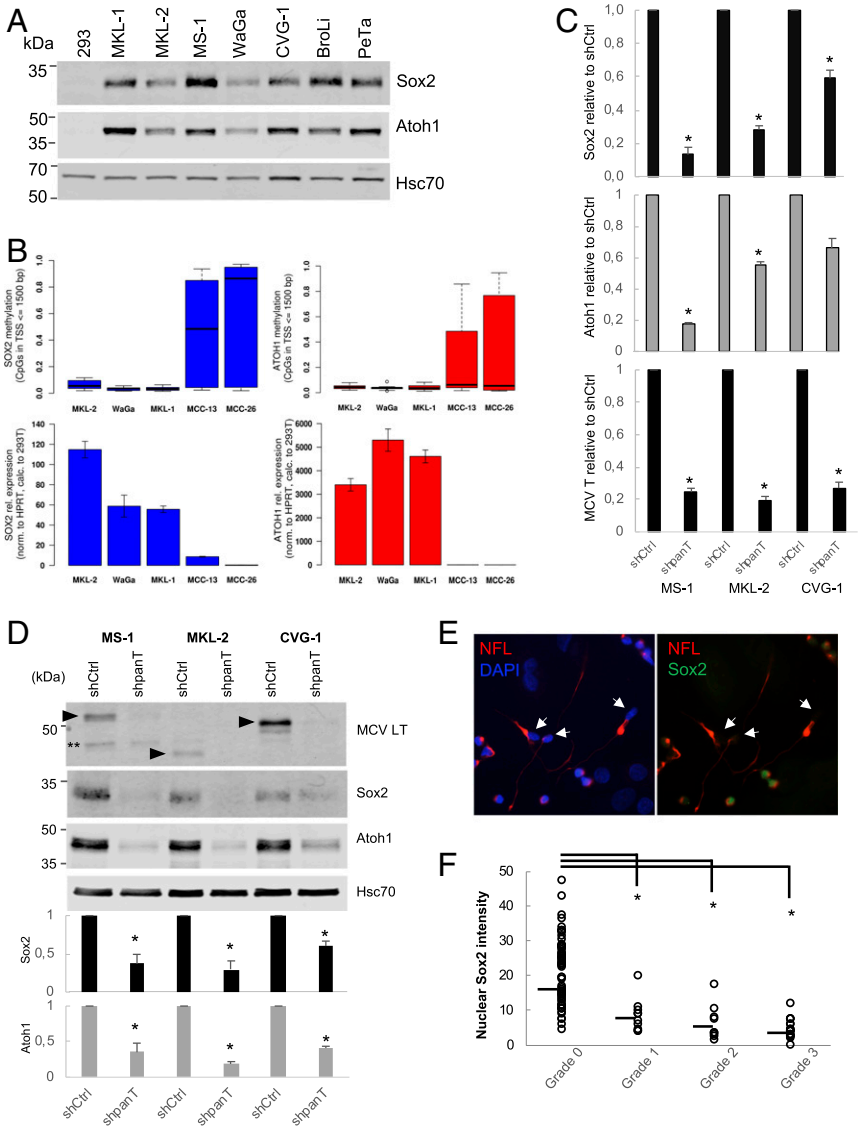

Fig. 4. MCV T antigen activates Sox2 and Atoh1 expression in MCC cells. (*A*) Sox2 and Atoh1 proteins are expressed in all MCV$^+$ MCC cells examined. (*B*) Hypomethylation of Sox2 and Atoh1 promoters is correlated with higher mRNA expression of Sox2 and Atoh1 in MCV$^+$ MCC cells. The number of CpG methylation sites in Sox2 or Atoh1 promoters counted within 1,500 bp upstream from the TSS are much lower in MCV$^+$ MCC cell lines (MKL-1, MKL-2, WaGa) than in MCV$^-$ cell lines (MCC-13 and MCC-26). The mRNA expression (*Lower*) was inversely correlated with CpG methylation levels. (*C*) T antigen knockdown decreases Sox2 and Atoh1 mRNA expression in MS-1, MKL-2, and CVG-1 cells. MCC cells transduced with shpanT-puro or shCtrl-puro were selected for 4 d with puromycin and grown in fresh medium without puromycin for 2 d. qRT-PCR was performed for Sox2, Atoh1, and MCV T antigen using 18S rRNA for normalization. The $2^{-\Delta\Delta CT}$ method was used to determine the relative mRNA abundance to shCtrl. Data are shown as average ± SD, $^*P < 0.05$ (Student *t* test). (*D*) Sox2 and Atoh1 protein expression is reduced by panT antigen knockdown in MS-1, MKL-2, and CVG-1 cells. Cells in *B* were subjected to LI-COR quantitative immunoblot analyses with Sox2 and Atoh1. An LT immunoblot confirms knockdown of T antigen by shpanT-puro. Closed arrowheads indicate truncated LT proteins. Hsp70 protein was detected as an internal control. Graphs indicate the quantitation of Sox2 and Atoh1 protein expression normalized by Hsp70. Data are shown as average ± SE, $^*P < 0.05$ (Student *t* test), Double asterisks (**) indicate nonspecific band. (*E*) Expression of nuclear Sox2 protein is attenuated in the differentiated MS-1 cells displaying grade 2/3 neurite formation (arrowheads). DAPI staining represents the location of nucleus. No Sox2 protein expression was detected from human keratinocytes used for coculture. (Magnification: 40×.) (*F*) Quantitation of Sox2 expression in different grade of neurite$^+$ cells. Sox2 protein expression was quantitated by ImageJ software. Values in *y* axis represent a nuclear Sox2 intensity after subtraction of a background. $^*P < 0.05$ (Student *t* test).

up-regulated by MCV T antigen in MCC. The expression of Atoh1 and Sox2 in MCC tissues has been reported previously (39, 40). In the 7 MCV$^+$ MCC cell lines examined, Sox2 and Atoh1 proteins were readily detectable by immunoblot (Fig. 4*A*). Methylation analyses performed for Sox2 and Atoh1 promoters revealed that CpG sequences within 1,500 bp from the transcription start sites (TSS) are hypomethylated in MCV$^+$ MKL-2, WaGa, and MKL-1 cells, whereas those in MCV$^-$ MCC cells, including MCC-13 and MCC-26, are highly methylated, consistent with high levels of Sox2 and Atoh1 mRNA expression in MCV$^+$ MCC cells (Fig. 4*B*). Sox2 has a distinct upstream region where MCV$^-$ MCC cells show more frequent CpG methylation than MCV$^+$ MCC cells (Chr 3 nucleotide position near 181,428,500) (*SI Appendix*, Fig. S4*A*). This region is only 1,000 bp upstream of the Sox2 TSS, thereby in perfect range to contain the promoter and well-conserved in vertebrates. Thus, CpG hypermethylation in this region may regulate the low Sox2 expression in MCV$^-$ MCC cells. CpG methylation in the Atoh1

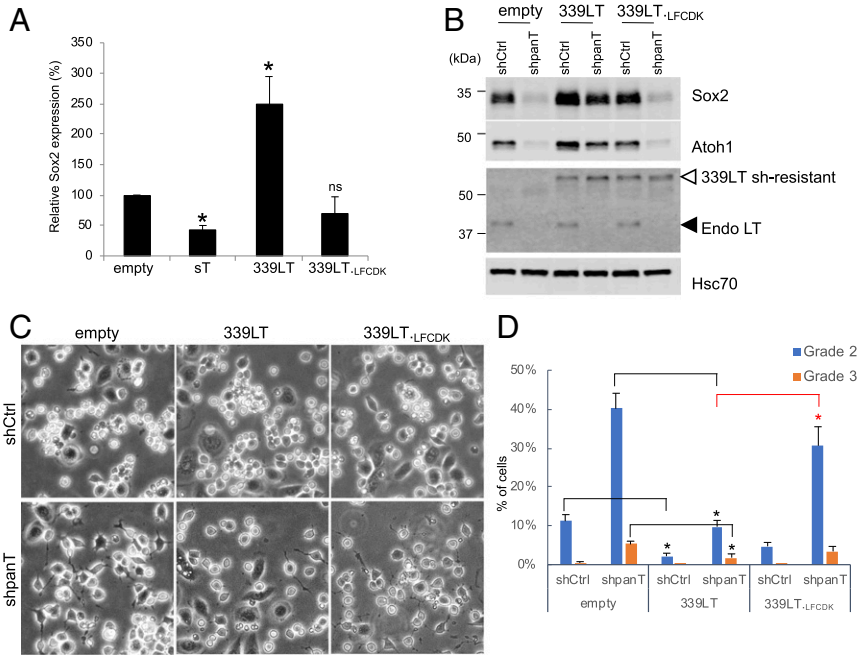

Fig. 5. The Rb-binding domain of MCV LT regulates both activation of Sox2 and Atoh1 and inhibition of neurite$^+$ cell formation. (*A*) Sox2 mRNA expression is induced by truncated tumor-derived LT isolated 339 (339LT) in human keratinocytes, but not by the Rb binding mutant (339LT.$_{LFCDK}$) or sT. Keratinocytes stably transduced with sT, 339LT, 339LT.$_{LFCDK}$, and control (empty) lentiviruses were subjected to qRT-PCR analysis for Sox2 using 18S rRNA for normalization. The $2^{-\Delta\Delta CT}$ method was used to determine the relative mRNA abundance to shCtrl. Data are shown as average ± SD, *$P < 0.05$ (Student *t* test). (*B*) Wild-type shRNA-resistant 339LT rescues Sox2 and Atoh1 expression under T antigen knockdown. MKL-2 cells stably transduced with codon-optimized 339LT, Rb-binding mutant 339LT.$_{LFCDK}$, and control vector were transduced with shCtrl-Neo or shpanT-Neo and selected with G418 for 6 d. After transduced cells were recovered in plain medium, cells were harvested for immunoblot to examine Sox2 and Atoh1 protein expression. (*C*) 339LT inhibits T antigen knockdown-induced MKL-2 differentiation. Cells in B were cocultured with keratinocytes for 5 d and photographed. (Magnification: 10×.) (*D*) MCC cell differentiation was evaluated according to the grading criteria in *SI Appendix*, Fig. S1*F*. Significance was determined through the comparison between empty and 339LT (black bars) and between 339LT and 339LT.$_{LFCDK}$ (red bars). Data are shown as average ± SE, *$P < 0.05$ (Student *t* test).

region is markedly lower in MCV$^+$ cells than in MCV$^-$ cells, and MCV$^-$ MCC exhibit more variation in their methylation levels compared to MCV$^+$ MCC (*SI Appendix*, Fig. S4*B*), suggesting that CpG methylation may influence Atoh1 expression in MCV$^-$ cells. When T antigen was knocked down in MS-1, MKL-2 and CVG-1 cells, Sox2 and Atoh1 mRNA expression was reduced, confirming the single-cell RNA sequencing results (Fig. 4*C*). In concordance with the mRNA expression, T antigen knockdown also resulted in reduced Sox2 and Atoh1 protein levels, as shown by immunoblot (Fig. 4*D*). When Sox2 and NFL proteins were stained in shpanT-transduced MS-1 cells under keratinocyte coculture, Sox2 expression was significantly reduced in the grade 1 to 3 neurite$^+$ cells, as compared to round MS-1 cells (grade 0) that retain high levels of nuclear Sox2 expression (Fig. 4 *E* and *F*), indicating that Sox2 expression is inversely associated with neurite formation induced by T antigen knockdown.

Viral LT Up-Regulates Merkel Cell Lineage Markers, Sox2 and Atoh1, and Inhibits Neurite$^+$ Cell Formation. To determine which T antigen isoform regulates Sox2 expression, we expressed codon-optimized MCV sT and tumor-derived truncated 339 large T (339LT) in keratinocytes (*SI Appendix*, Fig. S5*A*). qRT-PCR analyses demonstrated that MCV 339LT specifically increases Sox2 mRNA 2.5-fold (Fig. 5*A*). The induction of Sox2 mRNA was not observed when the Rb-binding mutant, 339LT.$_{LFCDK}$, was expressed, suggesting that the Rb-targeting of LT is essential for Sox2 induction. Next, the importance of LT expression on Sox2 expression was investigated in MCC cells. We transduced shRNA-resistant codon-optimized 339LT into MKL-2 cells to examine if exogenous LT expression rescues Sox2 expression upon endogenous T antigen knockdown. Both 339LT and 339LT.$_{LFCDK}$ were resistant to shpanT knockdown as expected, whereas endogenous 40-kDa LT protein was significantly reduced by shpanT (Fig. 5*B*). Under these conditions, wild-type 339LT rescued Sox2 expression when the endogenous T antigen was knocked down by G418-selectable shpanT-neo. We also observed the restoration of Atoh1 protein expression by wild-type 339LT, consistent with the LT regulation of Atoh1. In contrast, the 339$_{LFCDK}$ mutant rescued neither Sox2 nor Atoh1 protein levels (Fig. 5*B*). Using the same cells, we tested if exogenous LT expression affects neurite$^+$ cell formation induced by T antigen knockdown under keratinocyte coculture. Expression of wild-type 339LT markedly reduced neurite$^+$ cells in MKL-2 cells, regardless of T antigen knockdown, while 339$_{LFCDK}$ mutant did not show a significant effect (Fig. 5 *C* and *D*). Under T antigen knockdown, 339LT expression decreased grade 2 and grade 3 neurite$^+$ cells by 75% and by 65%, respectively, as compared to shpanT-transduced MKL-2 empty cells (Fig. 5*D*). A similar reduction in neurite$^+$ cell numbers by 339LT expression was also seen in MS-1 cells (*SI Appendix*, Fig. S5 *B* and *C*). We also found that human papillomavirus (HPV) 16 E7 inhibits neurite formation like 339LT. Expression of hemagglutinin (HA)-tagged E7 significantly reduced T antigen knockdown-induced neurite$^+$ cells in MS-1 cells. Expression of an Rb-binding mutant HA-E7.$_{LYCYK}$, however, did not inhibit neurite formation (*SI Appendix*, Fig. S5 *D* and *E*). Taken together, these results indicate that MCV LT expression, through its Rb-binding domain, promotes Sox2 and Atoh1 expression and suppresses the morphological conversion of MCC cells to neurite$^+$ cells.

Sox2 Directly Activates Atoh1 Expression and Is Essential for MCV$^+$ MCC Cell Proliferation and the Inhibition of Neurite$^+$ Cell Formation. The analysis of different MCV$^+$ MCC cell lines revealed that

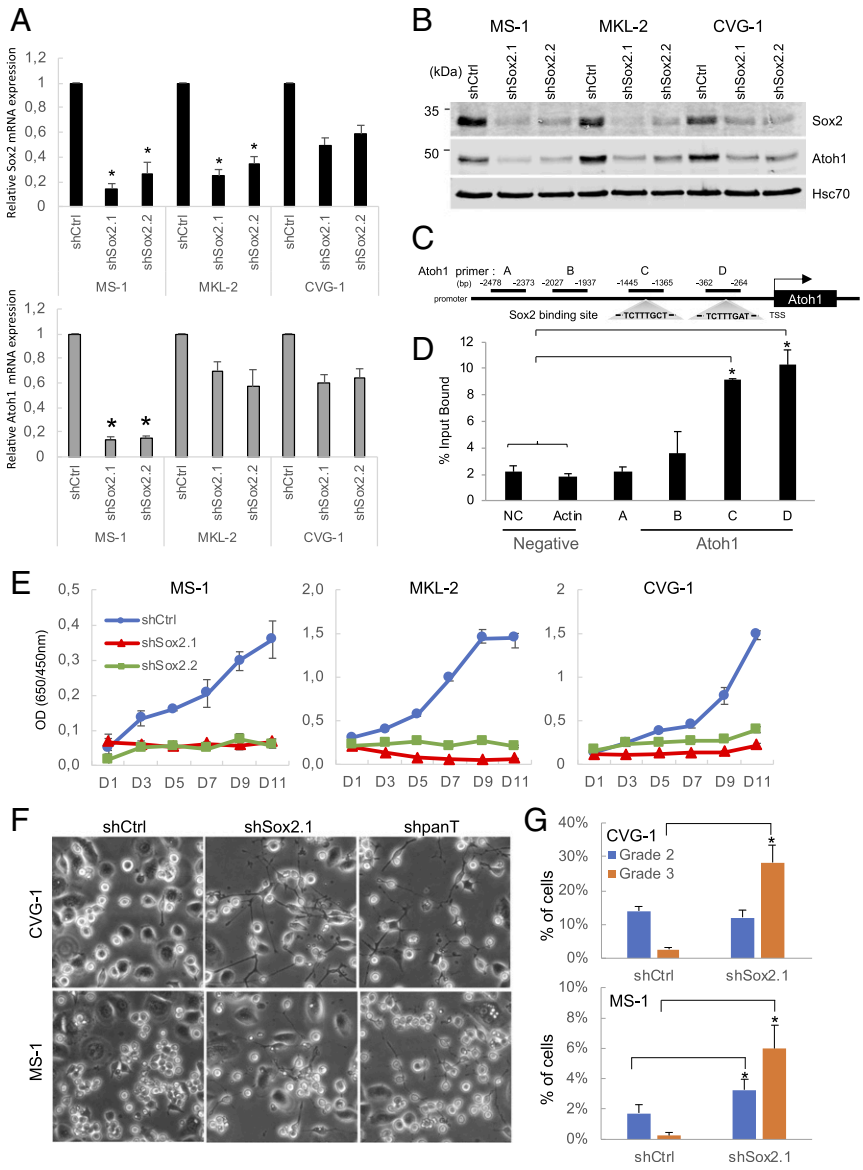

Fig. 6. Sox2 directly activates Atoh1 expression, promotes MCV$^+$ MCC cell proliferation, and inhibits neurite$^+$ cell formation. (*A*) Knockdown of Sox2 reduces Atoh1 mRNA expression. MS-1, MKL-2, and CVG-1 shCtrl-puro or 2 Sox2 shRNAs, shSox2.1-puro and shSox2.2-puro, were selected for 4 d and harvested at day 6 postinfection. Total RNAs were subjected to qRT-PCR analyses for Sox2 (*Upper*, black bars) and Atoh1 mRNA (*Lower*, gray bars) using 18S rRNA for normalization. Data are shown as average ± SD, $*P < 0.05$ (Student *t* test). (*B*) shRNA knockdown of Sox2 reduces Atoh1 protein expression. Samples harvested in *A* were subjected to immunoblot analyses to examine Sox2 and Atoh1 protein expression. Hsc70 was used as an internal control. The LI-COR Odyssey system was used to quantitate Sox2 (*Upper*, black bars) and Atoh1 (*Lower*, gray bars) protein expression with Hsc70 as a normalization control. (*C*) A schematic of the Atoh1 promoter region shows 2 potential conserved Sox2 binding sites upstream of the TSS, and 4 sets of qPCR primers are designed as indicated. (*D*) qPCR analysis of Sox2 ChIP at the promoter region of the Atoh1 gene shows the binding of Sox2 to sites C and D compared to negative control regions (NC: noncoding region and actin) in MKL-2 cells. Data are shown as average ± SE, $*P < 0.05$ (1-way ANOVA). (*E*) Knockdown of Sox2 ablates MCV$^+$ MCC cell proliferation. Three MCV$^+$ MCC cell lines with Sox2 knockdown in B were subjected to WST8 cell proliferation assays. (*F*) Like T antigen knockdown, Sox2 knockdown in CVG-1 and MS-1 increases neurite$^+$ cells similar to T antigen knockdown. (Magnification: 10×.) (*G*) Neurite$^+$ CVG-1 (F, *Upper*) or MS-1 (F, *Lower*) cells displaying grade 3 differentiation are significantly induced by shSox2.1-puro (*F*, *Center*), similarly to T antigen knockdown (*F*, *Right*). Differentiation was graded according to the criteria in *SI Appendix*, Fig. S1*E*. Data are shown as average ± SE, $*P < 0.05$ (Student *t* test).

Sox2 protein levels correlate with Atoh1 protein, but not with KRT20 (*SI Appendix*, Fig. S6 *A* and *B*). This result suggests that, as reported previously in normal Merkel cells (20), Sox2 may directly regulate Atoh1 expression in MCV$^+$ MCC cells. To examine this possibility, we knocked down endogenous Sox2 and investigated its effect on Atoh1 expression. When MS-1, MKL-2, and CVG-1 cells were transduced with 2 shRNAs, shSox2.1 and shSox2.2, Sox2 mRNA expression was knocked down markedly in MS-1 and MKL-2, and moderately in CVG-1 cells (Fig. 6 *A*, *Upper*). In the same samples, we also observed a moderate but concomitant decrease of Atoh1 mRNA expression, consistent with the Sox2 regulation of Atoh1 mRNA expression (Fig. 6 *A*, *Lower*). While Atoh1 mRNA reduction is moderate in MKL-2 and CVG-1 cells, the Atoh1 protein level was markedly decreased by 2 Sox2 shRNAs (Fig. 6*B*). To investigate the Sox2 regulation of the Atoh1 gene promoter, we then performed a chromatin immunoprecipitation (ChIP) assay. The Atoh1 promoter contains 2 Sox2 binding consensus motifs within 1,500 bp of the proximal promoter to the TSS (Fig. 6*C*). The ChIP experiment in MKL-2 cells demonstrated a 5-fold enrichment of Sox2 binding

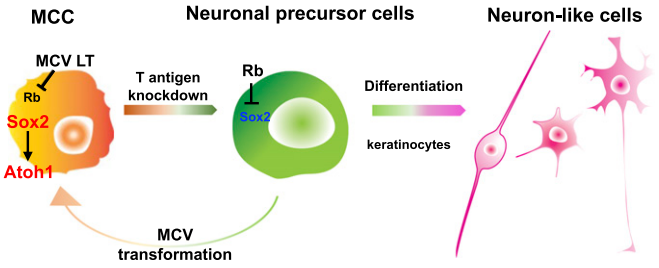

Fig. 7. A model of MCV$^+$ MCC genesis. Sox2, which is activated by MCV LT through the LXCXE Rb-binding domain induces Atoh1 and maintains tumorigenic state of MCC cells, inhibiting the phenotypic conversion of MCC cells to differentiated neuron-like cells. MCV may transform yet-to-be-defined neuronal precursor cells into Merkel cell-like cancer cells.

to the proximal Atoh1 promoter region (C and D) compared to the distal promoter region (A and B) or negative control regions (NC and actin) that do not contain predicted Sox2 binding sites (Fig. 6*D*). This Sox2 binding site is distinct from the previously defined mouse Atoh1 enhancer region that also contains Sox2 binding motifs (20). Taken together, these results indicate that Sox2 directly activates the transcription of the Atoh1.

Sox2 is an oncogene for cancers with stem cell properties, and its activity is essential for cancer stem cell (CSC) self-renewal or proliferation (41). We next examined if Sox2 functions as an effector of viral T antigen and contributes to tumorigenesis. Sox2 knockdown completely ablated the cell proliferation activities of all 3 MCV$^+$ cell lines (Fig. 6*E*). Since our results indicate Sox2 is an upstream regulator of Atoh1(Fig. 6 *B* and *D*), we knocked down Atoh1 alone to investigate the role of Atoh1 in MCC cell proliferation. The knockdown of Atoh1 protein expression by shAtoh1 was nearly 90% in MKL-2, but was moderate in MS-1 (50%) and CVG-1 (65%) cells (*SI Appendix*, Fig. S6*C*). Under these conditions, modest growth inhibition was observed in MS-1 and MKL-2, while no inhibition was seen in CVG-1 cells (*SI Appendix*, Fig. S6*D*). These data suggest that in MKL-2 and MS-1 cells, Atoh1 may also contribute to MCC cell proliferation as a downstream effector of Sox2; this notion is corroborated by our previous observation that increased Atoh1 expression correlates with aggressiveness of MCC (42).

Finally, we examined if the loss of Sox2 results in the formation of neurite$^+$ cells. When CVG-1 and MS-1 cells were transduced with shSox2.1 and cocultured with keratinocytes for 5 d, neurite$^+$ cells were significantly increased, as seen upon T antigen knockdown (Fig. 6*F*). The grade 3 neurite$^+$ cells were markedly increased, while we did not observe a significant increase for the grade 2 MCC differentiation (Fig. 6*G*). These data indicate that Sox2 is the key transcription factor that maintains the proliferative state of tumor cells and inhibits the morphological conversion to neurite$^+$ cells.

Discussion

Cellular transformation or immortalization induced by SV40 T antigen from a nonhuman primate polyomavirus is fully addicted to its oncoprotein expression. Thus, the tumorigenicity is reversible by the inactivation of its T antigen expression. Pancreatic β-cell tumors immortalized by SV40 LT can be reverted to functional β-cells in transgenic mice (43). Rat heart smooth-muscle cells, human hepatocytes, and human ensheathing glia cells, which are conditionally immortalized by SV40 T antigen, have also been shown to restore their cellular function with growth arrest upon the inactivation of T antigen (44–46). In this study, we examined whether human cancer, which was transformed by the first oncogenic polyomavirus MCV, can also be reverted to an untransformed state by the viral T antigen inhibition. Our current data indicate that 1) the Sox2–Atoh1 pathway activated by the Rb-binding domain of viral LT appears to be important for both the manifestation of a Merkel cell phenotype and tumorigenesis, and that 2) the in vitro inhibition of this pathway converts MCC tumor cells to differentiated neuronal cells, but not Merkel cells in the presence of cocultured keratinocytes (Fig. 7).

This study may also provide clues to a fundamental question: Why does MCV induce cancers with a Merkel cell phenotype? MCC is a neuroendocrine tumor, possessing gene-expression signatures similar to mechanoreceptor Merkel cells. Atoh1 and Sox2 are essential transcription factors that regulate Merkel cell development in mice. Atoh1 is a proneural transcription factor required for initial Merkel cell differentiation during Merkel cell development. The conditional knockout of Atoh1 in *Hoxb1*$^+$ skin epithelial and dermal cells in embryos ablates Merkel cells in mice (18). Sox2 also plays important roles in Merkel cell maturation and maintenance during embryonic Merkel cell development, and the conditional knockout of Sox2 in KRT14$^+$ embryonic epidermal cells significantly reduces Merkel cell numbers (19–21). Atoh1 and Sox2 are highly expressed in MCC tumors (40, 42, 47), thereby likely contributing to the manifestation of a Merkel cell-like phenotype in MCC tumors. The genomic amplification of *MITF*, a master regulator of melanocyte development, is critical for melanomagenesis (48). Thus, as *MITF* activation is linked to melanocyte lineage-specific transformation, the viral activation of the Sox2-Atoh1 oncogenic pathway could drive Merkel cell lineage-restricted carcinogenesis.

While the etiological role of MCV in MCC pathogenesis is clear, cells of MCC origin infected by MCV and transformed by MCV T antigen expression remain unknown. Initially, it was assumed that MCC tumors arise from transformed mechanoreceptor Merkel cells because of the ultrastructural and gene-expression similarities between normal Merkel cells and MCC (49, 50). Recent studies have proposed that the cellular origin of MCC may not be Merkel cells, and multiple cellular origins, such as epidermal stem cells or pro/pre-B cells were suggested for MCC (36, 51–53). Merkel cells are found at the basal layer of the epidermis and make synaptic contacts with nerve endings to form the Merkel cell–neurite complex for tactile sensing. In order to transmit signals to afferent nerves, Merkel cells fire action potentials by voltage-gated calcium channels (28) while voltage-gated sodium channels drive the action potential firing in most excitable cells. In our study, the T antigen knockdown not only decreased Sox2 and Atoh1 expression, but also developed neuronal but non-Merkel cell electrophysiological properties in neurite$^+$ cells, consistent with phenotypic conversion of MCC into neuron-like cells. These data suggest a possibility that MCC arises from precursor cells endowed with the potential to differentiate into neuron-like, but not Merkel, cells (Fig. 7).

MCC typically localizes within the dermis layer, and less than 10% of MCC are associated with the epidermis as seen in the rare cases of in situ MCC (54). This difference in tumor localization also infers that MCC may arise from different cells of origin (52, 55). Verhaegen et al. (56) reported transgenic mice that develop MCC-like tumors by expressing MCV sT and Atoh1 under the KRT5 promoter. Strikingly, the pathogenesis of MCC-like tumors in this model was confined to the epidermal layers, similar to in situ MCC or Merkel cell hyperplasia (57). These data suggests a possibility that a rare epidermal MCC known as in situ MCC may arise from Merkel cell precursors, whereas most of MCV$^+$ MCCs confined to the dermis may arise from neuronal precursor cells (58). Thus, it can be hypothesized that the dermis serves as the "stem cell niche" for the MCV-transformed neuronal precursor cells by preventing spontaneous differentiation stimulated by physical contact with the keratinocytes in the epidermis.

Initially, it was demonstrated that the knockdown of viral T antigen induces partial nonapoptotic cell death in MCV$^+$ cells (10). On the other hand, in the presence of keratinocytes, T antigen

knockdown promoted a phenotypic conversion of MCC cells to neuron-like cells, instead of inducing cell death. Since our results indicate that neurite outgrowth requires the presence of keratinocytes, cellular signaling from keratinocytes may support cell survival and the differentiation of T antigen knockdown cells into neuron-like cells. Further studies are needed to identify the keratinocyte-mediated cell signaling that promotes the neuron-like differentiation of MCC cells.

Our finding is consistent with recent results showing that the Rb tumor suppressor inhibits the expression of Sox2 and Oct4 and restricts cellular reprogramming as well as tumorigenesis (59). Rb has also been shown to be a repressor of cellular reprogramming and the development of CSCs (60). Tumor viruses have been suspected to target stem cells for transformation (61–63), and the Rb protein is commonly inhibited by tumor viruses (64). High-risk HPVs have been proposed to infect stem cells (65, 66). A recent study showed that HPV16 preferentially transforms basal keratinocytes with stem cell properties (67) and that the HPV E7 oncoprotein, which inhibits Rb similarly to MCV LT, activates pluripotency genes, including Oct4, Sox2, and Nanog (68). Thus, the targeting of cellular reprogramming factors, such as Sox2 and Oct4, may be a common mechanism for stem cell transformation by tumor viruses.

Sox2 can act as an oncogenic reprogramming factor and is expressed predominantly in cancer-initiating cells or CSCs (41). For many CSC-associated tumors, Sox2 is an essential oncogene and drives the self-renewal of transformed stem cells (41). If MCV$^+$ MCCs have properties similar to CSC-associated cancers, a specific therapy targeting the self-renewal of stem cells (e.g., therapies targeting Notch, WNT, and so forth) may be a fruitful direction of investigation.

Experimental Procedures

Coculture Experiments and Grading of Neurite Formation. Keratinocytes were seeded at 20% density in 6-well plates a day before the coculture experiment. Approximately 10^5 of MCV$^+$ MCC cells were washed with PBS once, suspended in keratinocyte medium, and transferred to the keratinocytes in a 6-well plate for coculture. At days 5 to 8 of coculture, the neurite outgrowth was graded from 0 to 3 according to its polarization and the relative neurite length to the cell body. Grade 0 represents no process, grade 1 cellular process-positive, grade 2 polarized projections, and grade 3 with projection longer than 2-cell body size. The neurite formation assays shown in Figs. 1*C*, 5*D*, and 6*G* and *SI Appendix*, Fig. S4 were evaluated by 4 different individuals. More than 250 cells were examined on the printed photographs in order to grade the neurite formation in a blinded and randomized fashion. Neurite$^+$ CVG-1 cells representing each grade (*SI Appendix*, Fig. S1*E*) were used as a reference when evaluated.

Statistics. Student's *t* test was used for qRT-PCR and neurite formation assays to determine statistically significant differences, and 1-way ANOVA was used for Sox2 ChIP experiments. Detailed materials and methods used for cell lines, plasmids, lentivirus production and infection, qRT-PCR, immunoblots, immunofluorescence, electron microscopy imaging, proliferation assays, whole cell patch clamp recording, single cell RNA sequencing and data analysis, DNA methylation analysis, and ChIP assay are provided in *SI Appendix, SI Experimental Procedures*.

ACKNOWLEDGMENTS. We thank Dr. Kathryn Albers, Dr. Paul Cantalupo, Dr. James Pipas, Dr. Patrick Moore, and Dr. Yuan Chang for critical advice and suggestions; and Michelle Savoldy, Navi Baskar, and Korey Henderson for technical assistance. This project used the University of Pittsburgh Health Science Core Research Facilities Genomic Research Core Single Cell RNA sequencing services. M.S. was supported by the Hillman Foundation, Pennsylvania Tobacco Settlement Grant P50CA121973, the University of Pittsburgh Skin Cancer Specialized Program of Research Excellence (SPORE), and National Institutes of Health Cancer Center Support Grant P30 CA047904. E.E. was supported by the Tisch Cancer Institute under P30 Cancer Support Grant and the Irma T. Hirschl Career Scientist Award of the Irma T. Hirschl Trust. J.C.B. was supported by the European Union's Seventh Framework Program (FP7-HEALTH-2011-two-stage, Immune Modulating Strategies for Treatment of Merkel Cell Carcinoma [IMMOMEC]) under Grant Agreement 277775 (granted to J.C.B.); J.C.B. was supported by the German Cancer Consortium (DKTK L441). The content is solely the responsibility of the authors and does not necessarily represent the official views of the National Institutes of Health.

1. D. W. Felsher, J. M. Bishop, Reversible tumorigenesis by MYC in hematopoietic lineages. *Mol. Cell* **4**, 199–207 (1999).
2. L. E. Dow *et al.*, Apc restoration promotes cellular differentiation and reestablishes crypt homeostasis in colorectal cancer. *Cell* **161**, 1539–1552 (2015).
3. C. S. Huettner, P. Zhang, R. A. Van Etten, D. G. Tenen, Reversibility of acute B-cell leukaemia induced by BCR-ABL1. *Nat. Genet.* **24**, 57–60 (2000).
4. I. Macpherson, Reversion in hamster cells transformed by Rous sarcoma virus. *Science* **148**, 1731–1733 (1965).
5. A. C. Maroney, S. A. Qureshi, D. A. Foster, J. S. Brugge, Cloning and characterization of a thermolabile v-src gene for use in reversible transformation of mammalian cells. *Oncogene* **7**, 1207–1214 (1992).
6. D. Ewald *et al.*, Time-sensitive reversal of hyperplasia in transgenic mice expressing SV40 T antigen. *Science* **273**, 1384–1386 (1996).
7. H. Feng, M. Shuda, Y. Chang, P. S. Moore, Clonal integration of a polyomavirus in human Merkel cell carcinoma. *Science* **319**, 1096–1100 (2008).
8. M. Shuda *et al.*, T antigen mutations are a human tumor-specific signature for Merkel cell polyomavirus. *Proc. Natl. Acad. Sci. U.S.A.* **105**, 16272–16277 (2008).
9. J. Cheng, O. Rozenblatt-Rosen, K. G. Paulson, P. Nghiem, J. A. DeCaprio, Merkel cell polyomavirus large T antigen has growth-promoting and inhibitory activities. *J. Virol.* **87**, 6118–6126 (2013).
10. R. Houben *et al.*, Merkel cell polyomavirus-infected Merkel cell carcinoma cells require expression of viral T antigens. *J. Virol.* **84**, 7064–7072 (2010).
11. R. Houben *et al.*, An intact retinoblastoma protein-binding site in Merkel cell polyomavirus large T antigen is required for promoting growth of Merkel cell carcinoma cells. *Int. J. Cancer* **130**, 847–856 (2012).
12. G. J. Starrett *et al.*, Merkel cell polyomavirus exhibits dominant control of the tumor genome and transcriptome in virus-associated Merkel cell carcinoma. *MBio* **8**, e02079-16 (2017).
13. H. Sihto *et al.*, Merkel cell polyomavirus infection, large T antigen, retinoblastoma protein and outcome in Merkel cell carcinoma. *Clin. Cancer Res.* **17**, 4806–4813 (2011).
14. P. J. Cimino *et al.*, Retinoblastoma gene mutations detected by whole exome sequencing of Merkel cell carcinoma. *Mod. Pathol.* **27**, 1073–1087 (2014).
15. M. Van Gele *et al.*, Gene-expression profiling reveals distinct expression patterns for classic versus variant Merkel cell phenotypes and new classifier genes to distinguish Merkel cell from small-cell lung carcinoma. *Oncogene* **23**, 2732–2742 (2004).
16. H. Haeberle *et al.*, Molecular profiling reveals synaptic release machinery in Merkel cells. *Proc. Natl. Acad. Sci. U.S.A.* **101**, 14503–14508 (2004).
17. M. B. Nguyen *et al.*, Dissection of Merkel cell formation in hairy and glabrous skin reveals a common requirement for FGFR2-mediated signalling. *Exp Dermatol.* **28**, 374–382 (2019).
18. S. M. Maricich *et al.*, Merkel cells are essential for light-touch responses. *Science* **324**, 1580–1582 (2009).
19. M. H. Lesko, R. R. Driskell, K. Kretzschmar, S. J. Goldie, F. M. Watt, Sox2 modulates the function of two distinct cell lineages in mouse skin. *Dev. Biol.* **382**, 15–26 (2013).
20. E. S. Bardot *et al.*, Polycomb subunits Ezh1 and Ezh2 regulate the Merkel cell differentiation program in skin stem cells. *EMBO J.* **32**, 1990–2000 (2013).
21. C. N. Perdigoto, E. S. Bardot, V. J. Valdes, F. J. Santoriello, E. Ezhkova, Embryonic maturation of epidermal Merkel cells is controlled by a redundant transcription factor network. *Development* **141**, 4690–4696 (2014).
22. C. Velásquez *et al.*, Characterization of a Merkel cell polyomavirus-positive Merkel cell carcinoma cell line CVG-1. *Front. Microbiol.* **9**, 713 (2018).
23. M. Shuda, H. J. Kwun, H. Feng, Y. Chang, P. S. Moore, Human Merkel cell polyomavirus small T antigen is an oncoprotein targeting the 4E-BP1 translation regulator. *J. Clin. Invest.* **121**, 3623–3634 (2011).
24. A. Guastafierro *et al.*, Characterization of an early passage Merkel cell polyomavirus-positive Merkel cell carcinoma cell line, MS-1, and its growth in NOD scid gamma mice. *J. Virol. Methods* **187**, 6–14 (2013).
25. E. M. Martin *et al.*, Parathyroid hormone-related protein, chromogranin A, and calcitonin gene products in the neuroendocrine skin carcinoma cell lines MKL1 and MKL2. *Bone Miner.* **14**, 113–120 (1991).
26. M. Pinget, E. Straus, R. S. Yalow, Localization of cholecystokinin-like immunoreactivity in isolated nerve terminals. *Proc. Natl. Acad. Sci. U.S.A.* **75**, 6324–6326 (1978).
27. R. A. Liddle, Cholecystokinin cells. *Annu. Rev. Physiol.* **59**, 221–242 (1997).
28. R. Ikeda *et al.*, Merkel cells transduce and encode tactile stimuli to drive Aβ-afferent impulses. *Cell* **157**, 664–675 (2014).
29. M. Shuda, H. J. Park, Y. Bai, Conversion of Sox2-dependent Merkel cell carcinoma to a differentiated neuron-like phenotype by T antigen inhibition. Gene Expression Omnibus. https://www.ncbi.nlm.nih.gov/geo/query/acc.cgi?acc=GSE136867. Deposited 4 September 2019.
30. A. P. Bracken, M. Ciro, A. Cocito, K. Helin, E2F target genes: Unraveling the biology. *Trends Biochem. Sci.* **29**, 409–417 (2004).
31. R. Arora *et al.*, Survivin is a therapeutic target in Merkel cell carcinoma. *Sci. Transl. Med.* **4**, 133ra56 (2012).
32. S. Hesbacher *et al.*, RB1 is the crucial target of the Merkel cell polyomavirus large T antigen in Merkel cell carcinoma cells. *Oncotarget* **7**, 32956–32968 (2016).

33. D. F. Condorelli *et al*., Glutamate receptor-driven activation of transcription factors in primary neuronal cultures. *Neurochem. Res.* **19**, 489–499 (1994).
34. J. Gu *et al*., Immunostaining of neuron-specific enolase as a diagnostic tool for Merkel cell tumors. *Cancer* **52**, 1039–1043 (1983).
35. I. Moll, F. Gillardon, S. Waltering, M. Schmelz, R. Moll, Differences of bcl-2 protein expression between Merkel cells and Merkel cell carcinomas. *J. Cutan. Pathol.* **23**, 109–117 (1996).
36. A. Zur Hausen, D. Rennspiess, V. Winnepenninckx, E. J. Speel, A. K. Kurz, Early B-cell differentiation in Merkel cell carcinomas: Clues to cellular ancestry. *Cancer Res.* **73**, 4982–4987 (2013).
37. S. A. Nicholson, M. B. McDermott, P. E. Swanson, M. R. Wick, CD99 and cytokeratin-20 in small-cell and basaloid tumors of the skin. *Appl. Immunohistochem. Mol. Morphol.* **8**, 37–41 (2000).
38. A. Van Keymeulen *et al*., Epidermal progenitors give rise to Merkel cells during embryonic development and adult homeostasis. *J. Cell Biol.* **187**, 91–100 (2009).
39. J. H. Leonard *et al*., Proneural and proneuroendocrine transcription factor expression in cutaneous mechanoreceptor (Merkel) cells and Merkel cell carcinoma. *Int. J. Cancer* **101**, 103–110 (2002).
40. A. C. Laga *et al*., Expression of the embryonic stem cell transcription factor SOX2 in human skin: Relevance to melanocyte and Merkel cell biology. *Am. J. Pathol.* **176**, 903–913 (2010).
41. A. Sarkar, K. Hochedlinger, The sox family of transcription factors: Versatile regulators of stem and progenitor cell fate. *Cell Stem Cell* **12**, 15–30 (2013).
42. T. Gambichler *et al*., Prognostic relevance of high atonal homolog-1 expression in Merkel cell carcinoma. *J. Cancer Res. Clin. Oncol.* **143**, 43–49 (2017).
43. S. Efrat, D. Fusco-DeMane, H. Lemberg, O. al Emran, X. Wang, Conditional transformation of a pancreatic beta-cell line derived from transgenic mice expressing a tetracycline-regulated oncogene. *Proc. Natl. Acad. Sci. U.S.A.* **92**, 3576–3580 (1995).
44. L. Jahn *et al*., Conditional differentiation of heart- and smooth muscle-derived cells transformed by a temperature-sensitive mutant of SV40 T antigen. *J. Cell Sci.* **109**, 397–407 (1996).
45. N. Kobayashi *et al*., Prevention of acute liver failure in rats with reversibly immortalized human hepatocytes. *Science* **287**, 1258–1262 (2000).
46. V. García-Escudero *et al*., A neuroregenerative human ensheathing glia cell line with conditional rapid growth. *Cell Transplant.* **20**, 153–166 (2011).
47. K. Heiskala, J. Arola, M. Heiskala, L. C. Andersson, Expression of Reg IV and Hath1 in neuroendocrine neoplasms. *Histol. Histopathol.* **25**, 63–72 (2010).
48. L. A. Garraway *et al*., "Lineage addiction" in human cancer: Lessons from integrated genomics. *Cold Spring Harb. Symp. Quant. Biol.* **70**, 25–34 (2005).
49. C. K. Tang, C. Toker, Trabecular carcinoma of the skin: An ultrastructural study. *Cancer* **42**, 2311–2321 (1978).
50. C. Toker, Trabecular carcinoma of the skin. *Arch. Dermatol.* **105**, 107–110 (1972).
51. G. Lemasson *et al*., Presence of putative stem cells in Merkel cell carcinomas. *J. Eur. Acad. Dermatol. Venereol.* **26**, 789–795 (2012).
52. J. C. Sunshine, N. S. Jahchan, J. Sage, J. Choi, Are there multiple cells of origin of Merkel cell carcinoma? *Oncogene* **37**, 1409–1416 (2018).
53. C. M. Sauer *et al*., Reviewing the current evidence supporting early B-cells as the cellular origin of Merkel cell carcinoma. *Crit. Rev. Oncol. Hematol.* **116**, 99–105 (2017).
54. H. A. Brown, D. M. Sawyer, T. Woo, Intraepidermal Merkel cell carcinoma with no dermal involvement. *Am. J. Dermatopathol.* **22**, 65–69 (2000).
55. P. W. Harms *et al*.; International Workshop on Merkel Cell Carcinoma Research (IWMCC) Working Group, The biology and treatment of Merkel cell carcinoma: Current understanding and research priorities. *Nat. Rev. Clin. Oncol.* **15**, 763–776 (2018).
56. M. E. Verhaegen *et al*., Merkel cell polyomavirus small T antigen initiates Merkel cell carcinoma-like tumor development in mice. *Cancer Res.* **77**, 3151–3157 (2017).
57. J. McFalls, L. Okon, S. Cannon, J. B. Lee, Intraepidermal proliferation of Merkel cells within a seborrheic keratosis: Merkel cell carcinoma in situ or Merkel cell hyperplasia? *J. Cutan. Pathol.* **44**, 480–485 (2017).
58. T. Ferringer, H. C. Rogers, J. S. Metcalf, Merkel cell carcinoma in situ. *J. Cutan. Pathol.* **32**, 162–165 (2005).
59. M. S. Kareta *et al*., Inhibition of pluripotency networks by the Rb tumor suppressor restricts reprogramming and tumorigenesis. *Cell Stem Cell* **16**, 39–50 (2015).
60. Y. Liu *et al*., Mouse fibroblasts lacking RB1 function form spheres and undergo reprogramming to a cancer stem cell phenotype. *Cell Stem Cell* **4**, 336–347 (2009).
61. R. Furuta *et al*., Human T-cell leukemia virus type 1 infects multiple lineage hematopoietic cells in vivo. *PLoS Pathog.* **13**, e1006722 (2017).
62. T. Jones *et al*., Direct and efficient cellular transformation of primary rat mesenchymal precursor cells by KSHV. *J. Clin. Invest.* **122**, 1076–1081 (2012).
63. H. Hu *et al*., Epstein-Barr virus infection of mammary epithelial cells promotes malignant transformation. *EBioMedicine* **9**, 148–160 (2016).
64. E. Bellacchio, M. G. Paggi, Understanding the targeting of the RB family proteins by viral oncoproteins to defeat their oncogenic machinery. *J. Cell. Physiol.* **228**, 285–291 (2013).
65. A. Schmitt *et al*., The primary target cells of the high-risk cottontail rabbit papillomavirus colocalize with hair follicle stem cells. *J. Virol.* **70**, 1912–1922 (1996).
66. J. Doorbar, Latent papillomavirus infections and their regulation. *Curr. Opin. Virol.* **3**, 416–421 (2013).
67. Y. Woappi, M. Hosseinipour, K. E. Creek, L. Pirisi, Stem cell properties of normal human keratinocytes determine transformation responses to human papillomavirus 16 DNA. *J. Virol.* **92**, e00331-18 (2018).
68. J. Organista-Nava *et al*., The HPV16 E7 oncoprotein increases the expression of Oct3/4 and stemness-related genes and augments cell self-renewal. *Virology* **499**, 230–242 (2016).